Frick, D. A., Schuessler, J. A., von Blanckenburg, F. (2016): Development of routines for simultaneous in situ chemical composition and stable Si isotope ratios analyses by femtosecond laser ablation inductively coupled plasma mass spectrometry. - *Analytica Chimica Acta*, *938*, pp. 33—43.

DOI: http://doi.org/10.1016/j.aca.2016.08.029

# Development of routines for simultaneous *in situ* chemical composition and stable Si isotope ratio analysis by femtosecond laser ablation inductively coupled plasma mass spectrometry

Daniel A. Frick[1*], Jan A. Schuessler[1], and Friedhelm von Blanckenburg[1,2]

[1] GFZ German Research Centre for Geosciences, 14473 Potsdam, Germany (*correspondence: dfrick@gfz-potsdam.de, +4933128828963)

[2] Institute of Geological Science, Freie Universität Berlin, 12249 Berlin, Germany

## Abstract

Stable metal (e.g. Li, Mg, Ca, Fe, Cu, Zn, and Mo) and metalloid (B, Si, Ge) isotope ratio systems have emerged as geochemical tracers to fingerprint distinct physicochemical reactions. These systems are relevant to many Earth Science questions. The benefit of *in situ* microscale analysis using laser ablation (LA) over bulk sample analysis is to use the spatial context of different phases in the solid sample to disclose the processes that govern their chemical and isotopic compositions. However, there is a lack of *in situ* analytical routines to obtain a samples' stable isotope ratio together with its chemical composition. Here, we evaluate two novel analytical routines for the simultaneous determination of the chemical and Si stable isotope composition ($\delta^{30}$Si) on the micrometre scale in geological samples. In both routines, multicollector inductively coupled plasma mass spectrometry (MC-ICP-MS) is combined with femtosecond-LA, where stable isotope ratios are corrected for mass bias using standard-sample-bracketing with matrix-independent calibration. The first method is based on laser ablation split stream (LASS), where the laser aerosol is split and introduced simultaneously into both the MC-ICP-MS and a quadrupole ICP-MS. The second method is based on optical emission spectroscopy using direct observation of the MC-ICP-MS plasma (LA-MC-ICP-MS|OES). Both methods are evaluated using international geological reference materials. Accurate and precise Si isotope ratios were obtained with an uncertainty typically better than 0.23 ‰, 2SD, $\delta^{30}$Si. With both methods major element concentrations (e.g., Na, Al, Si, Mg, Ca) can be simultaneously determined. However, LASS-ICP-MS is superior over LA-MC-ICP-MS|OES, which is limited by its lower sensitivity. Moreover, LASS-ICP-MS offers trace element analysis down to the µg $g^{-1}$-range for more than 28 elements due to lower limits of detection, and with typical uncertainties better than 15%. For *in situ* simultaneous stable isotope measurement and chemical composition analysis LASS-ICP-MS in combination with MC-ICP-MS is the method of choice.

## Keywords

femtosecond laser ablation, inductively coupled plasma multicollector mass spectrometry, split stream, optical emission spectroscopy, stable silicon isotope ratios

## 1. Introduction

### 1.1. The use of stable silicon isotopes in the Earth sciences

In the past two decades, novel isotopic tracers that fingerprint the distinct processes and the associated elemental mass fluxes occurring on Earth have been developed. The stable isotopes of metal (e.g. Li, Mg, Ca, Fe, Cu, Zn and Mo) and metalloid (e.g. B, Si, Ge) elements are today being explored as geochemical tracers to reveal insights into the detailed chemical reactions they were involved in. The stable isotope ratios shift during physicochemical reactions is preserved when a given element is transferred from one compartment into the other and this transfer is incomplete. Processes such as dissolution, precipitation, diffusion, or uptake into living cells are therefore accompanied by characteristic shifts in the isotope ratios.[1,2]

Silicon is the third most abundant element on Earth[3] and it occurs in the form of a wide variety of different rock-forming minerals, in dissolved form in aqueous environments, and as an essential constituent of biogenic silica utilised by various organisms and higher plants. Due to its crucial role in many geochemical and biogeochemical processes, Si is an ideal element to fingerprint process that entail mass-dependent isotope fractionation in the geo-, hydro- and ecosphere on Earth, as well as in extra-terrestrial environments. Various applications of Si stable isotopes are summarised in a recent reviews.[3–5] These include applications in oceanography, environmental sciences, plant physiology, igneous petrology, planetary sciences, and cosmochemistry. For many studies, the potential benefit of *in situ* micro-scale analyses are obvious. In meteorite studies, usually only a small amount of a specimen is available with large micro scale heterogeneities that contain important information on early interstellar processes (e.g., Ziegler *et al.*,[6]). In high temperature igneous petrology the Si isotopic fractionation between different micrometre-sized minerals in a rock disclose their origin and evolution history (e.g., Savage *et al.*,[4]). Moreover, at the Earth surface, complex low-temperature reactions cause chemical weathering of silicate rocks, leading to secondary mineral and soil formation on the one hand and to dissolved Si mass fluxes into rivers and eventually into the oceans on the other hand. This separation leads to complementary Si isotope signatures in both compartments (e.g., Opfergelt and Delmelle,[7] and Frings *et al.*[5]).

In fluid-solid interactions the chemical composition of both the solid and liquid phases are important controlling factors on Si isotope fractionation. Hence, the simultaneous determination of the silicon isotope composition and the chemical composition allows for a more comprehensive process understanding. In particular, the ability to analyse different phases in the same sample *in situ* at the micro-scale adds the textural context for interpretation. Methods for *in situ* silicon isotope ratio measurements exist, however not in combination with simultaneous chemical analysis.[8–10] Extending the capabilities to a more comprehensive elemental composition analysis has a huge potential for new scientific discoveries on micrometre scale samples. In this study we report two different approaches for evaluating *in situ* Si isotope ratio measurements with simultaneous determination of the chemical composition.

### 1.2. Analytical methods for *in situ* isotopic and elemental analysis

The *in situ* determination of the isotope composition of a solid sample can be achieved by two techniques, secondary ion mass spectrometry (SIMS) and laser ablation inductively coupled plasma multicollector mass spectrometry (LA-MC-ICP-MS). Whereas the achievable spatial resolution with SIMS (typically below 10 µm) is higher compared to LA-MC-ICP-MS, the demands on sample preparation and reference materials are higher for SIMS (e.g., see review by Wiedenbeck *et al.*[11]). Isotope ratio measurements have not yet been combined with simultaneous elemental analysis using only SIMS.

Laser ablation was first proposed by Gray as a sample introduction method for ICP-MS[12], and since then became the method of choice for *in situ* determination of the major and trace elements in solids[13]. However, one of the major sources uncertainty of quantitative laser ablation when using non-matrix matched standards for calibration, is laser induced fractionation.[14] Determination of *in situ* stable silicon isotope ratios was successfully achieved using nanosecond laser ablation.[15] Reducing the pulse length from nanoseconds to femtoseconds enables the quantification using non-matrix matched calibration materials[10]. This improvement is substantial for metallic and conductive samples but also for stable metal isotope analysis.[10,13,16,17]

Simultaneously determining the chemical composition and isotope ratio from a single ablation can be achieved in four different ways. (i) Measuring isotope ratios and chemical composition on a single instrument (e.g. single collector ICP-MS (ICP mass spectrometry), ICP-TOFMS (ICP-time-of-flight mass spectrometry) or ICP-M-H-MS (ICP-Mattauch-Herzog mass spectrometry)), (ii) splitting the laser aerosol and measuring the aerosol on dedicated, specialised instrumentation (laser ablation split stream (LASS) by combination of a multi and a single collector instrument [18]), (iii) a combination of laser induced breakdown spectroscopy (LIBS), where the elemental observation is made directly in the

laser plasma and LA-MC-ICP-MS[19] and (iv) optical emission spectroscopy using direct observation of the multicollector plasma to determine the chemical composition analysis[20].

Isotope ratios can be determined by means of single-collector ICP-MS. However, the precision attainable by these scanning instruments is acceptable for radiogenic or light stable isotope ratios (e.g. Li), but not sufficient to resolve the sub-permil isotope shifts of heavier stable metal and metalloid isotope ratios.[21] First reports about the prototype ICP-TOFMS (ToF Werke, Thun, Switzerland) indicate that the precision ($^{206}Pb/^{207}Pb$ 0.73% RSD, 10 µg $kg^{-1}$) is not sufficient to resolve the sub-permil variations in stable metal and metalloid isotope systems.[22] Results shown by Ardelt and co-workers from a new Mattauch-Herzog ICP-MS are promising in terms of accuracy.[23] However integration times of 40 to 100 s for a single replicate are not appropriate for transient laser ablation signals, and the background spectra shown by Resano *et al.* shows a large background elevation and depletion from the baseline, which could affect the elements of interest (e.g., Mg, Si and Fe).[24] In contrast, MC-ICP-MS is suited for high-precision isotope ratio analysis and can be combined with simultaneous element analysis. In static mode, the limited mass range covered by the multicollector array allows the simultaneous measurement of only a small number of elements (e.g., $^{23}Na$ up to $^{26}Mg$, $^{27}Al$ with $^{30}Si$). Fast dynamic scanning over a larger mass range is hampered by the instrument that is designed for high magnet stability, which is required for high resolution isotope ratio analysis. Therefore, using a single instrument to determine the isotope ratio and chemical composition at the same time is currently limited to very specific applications.

Splitting the laser aerosol towards different ICP mass spectrometers to simultaneously obtain precise isotope ratios and chemical compositions was first achieved by Yuan and co-workers.[18] In that study measurements of rare earth element abundances and U/Pb ages of single zircon grains on a single collector instrument were reported, while the hafnium isotope ratios were analysed simultaneously on a multicollector ICP-MS. The term LASS was established later by Kylander-Clark and co-workers, who determined U/Pb ages on a multicollector ICP-MS and rare earth element concentration on a single collector ICP-MS.[25] Since its first report in 2008, LASS became a routine technique to determine radiogenic isotopes and chemical composition of small or heterogeneous samples.[25] To our knowledge, however, LASS has never been applied to stable metal or metalloid isotope analysis with simultaneous chemical composition analysis.

Laser-induced breakdown-spectroscopy (LIBS) allows the simultaneous measurement of isotope ratios (by MC-ICP-MS) and chemical composition (by LIBS) without aerosol splitting. In LIBS, the sample is excited in the laser plasma and the emission spectra are used to determine the elemental concentrations in the sample.[26] Pioneering work combining LIBS and LA-ICP-MS has been published in the past years.[19,27] However, one of the major limitation of LIBS is the strong matrix dependency of the signal intensities, meaning that calibration without a matrix-matched standard is difficult, while for calibration-free LIBS some plasma-related properties need to be determined.[26]

Recently, optical emission spectroscopy using the analytical plasma of the MC-ICP-MS has been used to simultaneously analyse boron isotope ratios and B/Ca ratios in marine carbonates.[20] The beauty of this approach lies in its simplicity - the laser aerosol is transported into the multicollector ICP source, where the isotope ratios are determined, while the light emission from the plasma is analysed by an optical spectrometer and hence the chemical composition is also determined.

To simultaneously determine silicon isotope ratios and the chemical composition of a sample either laser aerosol split stream (LASS) or optical emission spectroscopy on the multicollector plasma are feasible. These two approaches are evaluated in the following using geological reference materials. First, two possibilities of collecting the light from the multicollector plasma are evaluated. Second, LASS in combination with a quadrupole ICP-MS and rear-on light collection OES (LA-MC-ICP-MS|OES) are evaluated.

## 2. Materials and methods

### 2.1. Instrumentation

#### 2.1.1. Laser ablation

For matrix-independent Si isotope determination, the use of a femtosecond laser ablation system (fs-LA) provides considerable advantages over nanosecond-LA (ns-LA).[10] The use of ns-LA leads to composition-dependent instrumental mass bias. Unknown samples therefore need to be measured against matrix-matched reference materials.[28] The laser ablation system used in this study has been described in detail by Schuessler and von Blanckenburg.[10] Briefly, a UV fs-LA system (Spectra Physics Solstice, USA) in combination with a petrographic microscope and a custom-built stage and laser software for automated analysis are used. The fs-pulse generation is based on a Ti:sapphire seed laser, which is amplified using the chirped pulse amplification method, pumped by a Nd:YLF laser. The resulting IR beam ($\omega$ = 785 nm, up to 3.5 mJ/pulse) is frequency-doubled ($2\omega$ = 393 nm) and successively frequency-tripled ($3\omega$ = 262 nm). The third harmonic is frequency-summed in a nonlinear combination with the fundamental wavelength to obtain 196 nm. This deep-UV beam is focused through an achromatic lens-triplet onto the sample surface. In order to avoid laser plasma breakdown, care was taken during the set-up of the LA system to position the focus of the laser beam beneath the sample surface.[29] The typical laser settings used throughout the experiments are shown in Table S1 in the Supplementary Information. The laser aerosol is transported through polytetrafluoroethylene lined tubing (Tygon SE-200, Saint Gobain) into the ICP-MS. Helium was used as transport gas and Argon was added just before the ICP.[30,31]

#### 2.1.2. Multicollector ICP-MS

Silicon isotope ratios were determined on a high-resolution multicollector ICP-MS (Neptune, with Jet Interface upgrade, Thermo Fisher Scientific, Germany). To resolve isobaric interferences (mainly $^{14}N^{16}O^{+}$ on $^{30}Si^{+}$) the ion optics were operated at medium mass resolution with a typical mass resolving power $m/\Delta m > 5000$. Faraday detectors (equipped with $10^{11}$ Ω amplifiers) were positioned to obtain interference free, flat top peak shoulders. The Faraday cup configuration is shown in Table S2. The gas flows, torch position and ion optics were tuned daily for highest intensity and mass bias stability, while maintaining the $^{14}N^{16}O^{+}$ interference on $^{30}Si^{+}$ at reasonably low levels (<10 V). The addition of water during non-matrix matched quantification using laser ablation has proven to be advantageous, e.g. [31–33]. The addition of water leads to a similar condition of the highest analyte ionisation density in the plasma regardless of the matrix, and therefore leads to an improved accuracy in non-matrix matched quantification.[34,35]. The make-up argon which is added to the laser aerosol is thus moisturised using ultrapure water by passing through a 50 µL $min^{-1}$ PFA nebuliser and a combined cyclone-Scott double pass spray chamber. Water and laser aerosol were mixed using a Y-piece before entering the ICP torch of the mass spectrometer.

To avoid isotope fractionation during LA sampling, transport and ionisation, three measures are taken: the use of fs-LA improves the matrix-independent calibration capabilities (see [10] and discussion therein), the addition of water to the plasma increases the robustness of the plasma (see [31–35]) and matching the ion beam intensities between samples and bracketing standards assures similar plasma loading (see [10] and discussion therein). All three measures together enables to determine, accurately and precisely, the Si isotopic composition, using a non-matrix matched standard sample bracketing approach.[10] The ion beam intensities between samples and bracketing standards were matched by individually adjusting the LA frequency.

#### 2.1.3. Quadrupole ICP-MS

The chemical composition of the split laser aerosol was determined by a quadrupole ICP-MS (iCAP-Qc, Thermo Fisher Scientific, Germany). The ICP-MS was tuned daily for highest sensitivity on NIST SRM610, while maintaining a $^{238}U/^{232}Th$ ratio close to 1 and a $^{238}U^{16}O/^{238}U$ ratio below 0.7%.[12, and Ref. therein] To keep the oxide formation rate low, no water was added to the quadrupole ICP-MS.

#### 2.1.4. Light collection OES

Collecting the emission light from the multicollector plasma and introducing it into an optical spectrometer enables simultaneous Si isotope and element concentration analysis using a single plasma source. The advantage is that all the ablated material is introduced into the MC-ICP-MS. [20] Commercial ICP-OES instruments use both radial and axial plasma observation. The radial set-up is preferred for complex matrices, since the observation height can be adjusted and thus interferences can be avoided. The axial plasma observation, however, shows higher sensitivity due to integration over the entire plasma length. Axial plasma view from the front (as realised in commercial ICP-OES instruments) is not accessible if, as in the setup presented here, the ion beam is extracted into the MC-ICP-MS. Thus, the light of the plasma was either collected side-on (see upper part of Figure 1) or rear-on through the injector (see lower part of Figure 1). The light was coupled into a fibre bundle (19 fibres, Ø=1.3 mm, BF13HSMA02, ThorLabs, Germany) using an UV-fused silica plano-convex lens (f=35.1 mm, LA4052, ThorLabs, Germany). Side-on viewing was achieved by removing both windows on the instrument housing (outer observation glass and inner metal mesh) and positioning the collection lens at the inner torch housing window (see upper part of Figure 1). The light was collected through the small gap of the platinum guard electrode surrounding the torch. For a safe positioning of the optics during plasma operation, spindles were added to a kinematic mount and operated outside the torch box. For rear-on observation through the injector, the focusing optic was placed behind a laminar flow adapter made of quartz glass. The tangential entry of the laminar flow adapter was used to add the aerosol (laser aerosol and ultrapure water) to the plasma, whereas the straight axial entry was closed at one side using a silicate glass cover slip. The other end of the fibre bundle was placed in the torch box of the OES, and positioned where in the original set-up the tip of the inner plasma tail is. The used OES is an axial ICP-OES (Varian 720-ES, Varian, Australia), featuring a high resolution echelle polychromator and CCD detector with the capabilities to simultaneously measure the wavelength range from 167 to 785 nm. The x-y mirrors behind the cone of the OES were optimised for highest intensity on an Ar emission line (Ar 420.067 nm). Both set-ups were compared in terms of sensitivity and limits of detection. This approach allows us to use the OES instrument without any modification, and switching over from OES to ICP-OES can be done within minutes. Table S3 shows the instrument settings for the multicollector ICP-MS and the OES, schematics of the side-on and rear-on OES set-up are shown in Figure 1.

For are more routine application a second OES instrument was stripped down, using only the parts of the optical emission spectrometer, without the ICP and the sample introduction system. This allows to place the fibre bundle close to the spectrometer shutter. Using a commercial ICP-OES offers the advantages of a technically mature software package including: automatic wavelength calibration and a vast library of different atomic and ionic emission lines, their relative intensities and indication of potential interferences. The software further allows to perform background subtraction, standardise results and automatically trigger the start of the analysis by an external source, e.g. the laser.

### 2.2. Simultaneous combination of chemical composition and isotopic ratios

In initial experiments, we tested LASS combined with ICP-OES and found indeed more than 10 elements (Li, Be, Na, Mg, Al, Si, Ca, Ti, Mn, Fe and Sr) were above background for NIST SRM610. However, their detection limits ranges between $10^2$ µg $g^{-1}$ (Sr) and $10^5$ µg $g^{-1}$ (Si) which is 1.5 to 3 orders of magnitude higher than LASS in combination with quadrupole ICP-MS. LASS-ICP-MS is superior in terms of the elemental scope and limits of detection and thus the LASS combination with ICP-OES was not further pursued.

#### 2.2.1. Laser ablation split stream in combination with an ICP-MS (LASS-ICP-MS)

The laser aerosol was split at the outlet of the laser ablation cell and introduced into two instruments, a multicollector ICP-MS and a quadrupole ICP-MS. To control the amount of aerosol transported into the quadrupole ICP-MS the concept developed by Glaus *et al.* was adapted.[36] A small amount of the laser aerosol was actively pumped out of the helium stream using a diaphragm pump (NMP 05, KNF,

Germany). Figure 2 shows a schematic LASS ICP-MS setup, the used instrument settings are given in Table S4.

#### 2.2.2. LA-MC-ICP-MS with light collection optical emission spectroscopy (LA-MC-ICP-MS|OES)

Optimisation of the fibre optics positioning for light collection was performed using solution nebulisation and a 2 µg $g^{-1}$ multi element solution (ICP multi-element standard solution IV, Merck KGaA, Germany with Be, Si and Ti added) under laser ablation conditions (helium added through the ablation cell). Two different strategies of collecting the emitted light, rear-on and side-on, are compared (see section 2.1.4). The more sensitive and versatile strategy (rear-on LA-MC-ICP-MS|OES) is then compared with LASS-ICP-MS.

### 2.3. Samples

To compare and evaluate the different analytical routines a selection of geological reference materials was used. The choice of samples (see Table 1) was made based on differences in their absorption behaviour, broad variation of silicon content and the availability of reference values (in particular for $\delta^{30}Si$). Concentration and isotopic composition for the reference materials were taken from Jochum *et al.*[37],the GeoReM database[38] and Schuessler and von Blanckenburg[10].

### 2.4. Quantification

#### 2.4.1. Elemental concentration

Data evaluation for chemical composition analyses by LA-ICP-MS was carried out in StalQuant, a Phyton-based program to reduce large numbers of point-by-point quantification data developed by the Günther Group, ETH Zürich.[39] NIST SRM610 was used as external standard, while differences in the ablation yield were corrected using either an internal standardisation[40] or a 100% weight oxide[41] normalisation approach. Modification to the original StalQuant code was made to allow direct import of iCAP-Qc data. OES data was exported as a single csv file, and rearranged using a custom written bash script (see Supplementary Information). Limits of detection, concentration of the unknown sample and accuracy of reference materials were calculated in a spreadsheet. For LA-MC-ICP-MS|OES Ca (396.847 nm) was used as internal standard. Limits of detection are based on three times the standard deviation of the gas background.[40]

The intensities obtained for $^{27}Al$ and $^{28}Si$ on the MC-ICP-MS were also used to quantify those elements. The intensity of Ca (396.847 nm), determined by LA-MC-ICP-MS|OES, is used as internal standard to correct for different ablation yield and the concentration of Al and Si are calculated according to the procedure from Longerich *et al.*[40]

#### 2.4.2. Si isotope ratios

One of the main challenges in determining accurate stable isotope ratios is the need to correct the instrumental mass bias. Whereas in the analysis of radiogenic isotopic ratios the mass bias can be corrected relative to an internal isotope ratio that is defined as being invariant, this is not possible for stable isotope ratios systems, where the aim is to determine the natural variations of all ratios. As the instrumental mass bias affects all stable isotope abundances of the element, an external mass bias correction is needed.[10] One possibility is to use the standard-sample-bracketing approach, where a linear trend between the standards analysed before and after the sample is assumed.[42] The variations in the stable Si isotope compositions observed in nature are very small and are typically reported in the δ notation as permil deviation (see equation 1) relative to an international measurement standard (NIST 8546 aka NBS28, $\delta^{29}Si \equiv 0‰$ and $\delta^{30}Si \equiv 0‰$).[43] NBS28 is a fine-grained quartz sand that is cumbersome to use as bracketing standard, since line scans need to be adapted to individual grain shapes. Instead we used NIST SMR610 as bracketing standard. As the two, NIST SRM610 and NBS28, are isotopically identical, we do not expect any differences to the data reported relative to NBS28. Every analytical session consisted of only a few analyses of NBS28 relative to NIST SRM610, to confirm the isotopic agreement between them. All silicon isotope ratios in this work are reported relative to NIST SRM610 and no recalculation relative to NBS28 was performed. Isotope ratios

were evaluated using a custom written spreadsheet (see Schuessler and von Blanckenburg for details [10]).

$$\delta^{30}Si = \left[ \frac{\left(\frac{^{30}Si}{^{28}Si}\right)_{Sample}}{\left(\frac{^{30}Si}{^{28}Si}\right)_{NIST610}} - 1 \right] [in\ ‰] \quad (1)$$

## 3. Results and discussion

In this section first the results obtained by rear-on and side-on LA-MC-ICP-MS|OES are evaluated, also with respect to ease of use of the proposed routine. Second, LASS-ICP-MS and rear-on LA-MC-ICP-MS|OES are compared considering their capabilities in simultaneous chemical analysis and isotopic ratio determination.

### 3.1. Comparison between rear-on and side-on LA-MC-ICP-MS|OES

Both setups, rear-on (collecting the light through the injector) and side-on (diagonal plasma observation through the gap in the platinum guard electrode mounted on the torch of the MC-ICP-MS) were compared. For better reproducibility (day-to-day differences in the laser performance) and for assessing a broader range of elemental concentrations, measurements with both setups were done with solution nebulisation using a 2 µg $g^{-1}$ multi element solution, rather than laser ablation. The results of the limits of detection based on 3 times the standard deviation of a 1% $HNO_3$ blank are shown in Figure 3.

No clear difference is apparent between the two plasma observation methods. Rear-on OES shows lower limits of detection for a majority of the investigated elements and emission lines. However, for emission lines in the deep UV range (Be 313.042, Fe 259.940, Si 251.611, Si 288.158 and Zn 334.502, in nm), side-on OES is advantageous. The higher limits of detection for rear-on OES can be explained by absorption of light by water vapour and the laser aerosol passing through the injector, and the relatively long and narrow optical path from which the emission light is collected. Nevertheless, the more practical day-to-day handling of the rear-on OES set-up (when switching between different sample introduction systems on the MC-ICP-MS) outweighs the lower limits of detection in the deep UV and is used throughout the rest of this study. Furthermore, for rear-on OES, no modification to the torch box is needed, and no metal-jacketed optical fibres are placed in close proximity to the plasma source.

### 3.2. Comparison between rear-on LA-MC-ICP-MS|OES and LASS-ICP-MS

In the following, we compare four LASS-ICP-MS and three rear-on LA-MC-ICP-MS|OES sessions in terms of their scope for elemental concentration measurements, Si isotope ratio measurements, and their accuracy and precision as determined by repeated measurements on reference materials. With these results we will show that rear-on |OES is impaired by high limits of detection, and that Si isotope ratio accuracy and precision are not affected when using only a small fraction of the aerosol for the quadrupole ICP-MS in LASS-ICP-MS.

#### 3.2.1. Elemental scope and limits of detection

The elemental scope and limits of detection (LOD) of LA-MC-ICP-MS|OES and LASS-ICP-MS are shown in Figure 4. Whereas for LA-MC-ICP-MS|OES only the major elements in NIST SRM610, Na, Al and Ca, are above the background, the majority of the ICP-MS detectable elements in LASS-ICP-MS are above the LOD. LODs for most of elements are in the tens of µg $g^{-1}$ or better. Since quadrupole ICP-MS was operated without using the collision cell to remove spectral interferences, some elements (e.g. Al, Si, P, K, Ca and Fe) show higher LODs. The clearly visible day to day variations of the LODs (see Figure 4) are due to the individual adjustment of the aerosol split flow between the MC-ICP-MS and the quadrupole ICP-MS. These were adjusted to assure optimal conditions for the silicon isotope ratio

determinations. For the analytical session number 3 the split towards the MC-ICP-MS had to be increased due to prior installation of new high-resolution entrance slits and thus the amount of aerosol reaching the quadrupole ICP-MS was reduced (see also discussion in 3.2.2).

#### 3.2.2.Chemical composition analysis

The results from the matrix-matched quantification for NIST SRM612 and SRM610, using NIST SRM610 as bracketing standard, are shown in Figure 5 and Supporting Figure 1, respectively. Whereas for LASS-ICP-MS a major part of the elements of the periodic table can be detected, for rear-on OES only Al, Ca, Na and Si were above the background (see panel c of Figure 5). These elements are present in high concentrations in the NIST SRM61x glasses. Other results are likely from samples with different chemical composition, like natural rocks/glasses, or sulphide and oxide minerals. The restrictions of rear-on OES in terms of limits of detection has several reasons. First, the small diameter through which the plasma was observed is limiting the light collection. Second, the long distance between the plasma source and the collection lens (approximately 25 cm) is accompanied by loss in the light intensity. Third, part of the collected light was scattered before the spectrometer entrance.

No significant deviations between the different standardisation approaches were observed for LASS-ICP-MS (Figure 5 panel a-b). Using $^{29}$Si as internal standard or applying the 100 wt% oxide-normalisation both gave accurate (typically better than 10-15%) and precise (typically 5-10%) results. Since no chemical reaction or physical mass resolution technology was used to supress molecular interferences (e.g. collision cell), higher deviations from the reference value for $^{31}$P, $^{39}$K and $^{56}$Fe were observed, especially in the low-concentrated NIST SRM612. In rear-on OES matrix-matched quantification was possible for the four elements above detection limit using Ca (396.847 nm) as internal standard.

The scope of detectable elements for rear-on LA-MC-ICP-MS|OES can be extended using the signal intensities of $^{27}$Al and $^{28}$Si obtained from MC-ICP-MS to calculate the content in the sample (see Figure 5 panel c, $^{27}$Al and $^{28}$Si).

As an example for non-matrix matched quantification results of ATHO-G (rhyolite glass) and BHVO-2G (basalt glass) are shown in Figure 6 and Figure 7, respectively. For ATHO-G analysed by LASS most of the elements are accurate within 10-15% (Figure 6a-b). However, since only a small part of the aerosol is transported into the quadrupole ICP-MS, certain elements are below the limits of detection (e.g. $^{31}$P, $^{45}$Sc and $^{208}$Pb). These elements would be above background in direct LA-ICP-MS (without aerosol splitting). The slightly higher deviation observed for $^{23}$Na is within the reported uncertainty for ATHO-G (see Borisova *et al.* and values reported in the GeoReM database [38,44]).

For samples that show large differences in their chemical composition relative to the reference standard, rear-on LA-MC-ICP-MS|OES shows reduced achievable accuracy and precision. Accuracy for Ca (422.673 nm) is well outside the ±40% limit (Figure 6c). Larger deviation from the reference values are also observed for the quantification of $^{27}$Al and $^{28}$Si intensities obtained from the multicollector ICP-MS analyses using Ca (396.847 nm) from the |OES as internal standard. Thus, for samples where large deviation between the internal standard concentrations are observed, Ca (396.847 nm) is not an optimum internal standard to correct ablation yields on the MC.

For BHVO-2G (Figure 7) similar results as for ATHO-G are observed. Major elements for LASS-ICP-MS are accurate within 10-15%, while for rear-on OES higher deviations for Al (396.152 nm) and Na (588.995 nm) were observed. Prior to the analytical LASS session #3 the high resolution entrance slits of the multicollector instrument were renewed, thus a larger fraction of the laser aerosol was introduced into MC-ICP-MS to compensate for the lower transmission through the narrower slit. Hence, similar signal intensities compared to previous analytical sessions were obtained. This adjustment is done so that the amount of ablated material does not need to be increased. This partitioning, however, is done at the expense of higher limits of detection for trace elements quantification on the remaining aerosol amount directed towards the quadrupole ICP-MS. Therefore,

the limits of detection for quadrupole ICP-MS were higher resulting in a higher uncertainty and an inferior precision for the elements that are low in concentration.

Similar results for GOR128-B and T1-G can be found in Supporting Figure 2, and Supporting Figure 3, respectively.

#### 3.2.3.Si isotope ratios

For the analytical sessions reported in the previous section the stable silicon isotope ratios were determined simultaneously and results are shown in Figure 8. NBS28 was analysed as an unknown sample and bracketed against NIST SRM610. No significant difference between SRM610 and NBS28 was observed, which is in agreement with the data reported in the literature (see Schuessler and von Blanckenburg and the GeoReM Database [10,38]).

Results for matrix-matched bracketing, NIST SRM610 and SRM612, are well within the reported values in the literature. No systematic difference between fs-LA [10], fs-LASS and rear-on LA-MC-ICP-MS|OES in terms of the accuracy and precision was observed. We do not expect LA-MC-ICP-MS|OES to differ from fs-LA-MC-ICP-MS that without simultaneous chemical measurement, as the isotope ratio measurement-setup is identical in both experiments. Our isotope ratio measurement results also agree with literature values for non-matrix matched bracketing of ATHO-G, BHVO-2G and T1-G (see Figure 8) and GOR128-G and IRMM017 (see Supporting Figure 4).

All Si isotope results determined by LASS-ICP-MS and LA-MC-ICP-MS|OES are shown in Table 2. Comparing single analytical sessions small differences in the repeatability (based on 2 SD) between LASS and rear-on OES were observed (e.g. LASS number 1 and rear-on OES number 3 for T1-G, 0.43 vs. 0.24, respectively, see Figure 8). However, there is no overall trend in the entire dataset. It is encouraging to find that isotope ratio measurements with LASS resulted on average in similar precision when compared to the precision achieved during fs-LA-MC-ICP-MS analysis, even though a small part of the laser aerosol was physically split. This finding indicates that the precision of the isotopic analysis is not affected by the small amount removed from the aerosol stream as long as the total amount of ions reaching the multicollector is close to or above 7 V on $^{28}Si$ and sample and bracketing standards are intensity matched within ± 25%.[10]

Our directed split stream approach, using a pumped flow towards the quadrupole ICP-MS is superior to an undirected flow. Pumped split flow ensures that the optimum amount of laser aerosol is reaching the multicollector ICP-MS. In the LASS-ICP-MS session number 3 the amount of laser aerosol reaching the MC-ICP-MS had to be increased due to new high mass resolution slits, hence the chemical composition analysis suffered from higher LOD (see Figure 7 and discussion thereof). However, no significant difference in the accuracy between the analytical sessions for BHVO-2G is observed. Thus the advantage of the pumped split flow is demonstrated.

Introducing a device (i.e. a pump) into the laser aerosol path could lead to a contamination of the transported aerosol, slow down the washout or lead to particle trapping. During the evaluation neither of those problems were observed. Possible contamination or carry over during the analytical sessions were not observed. The background for silicon and the other elements were stable. The laser ablation cell is optimised for stable isotope ratios, thus for stable signal and not for fast washout. An increase in the washout time due to the pump was not observed.

## 4. Future perspectives

LASS-ICP-MS is in routine use in our laboratory to determine the chemical and isotopic composition of weathered mineral phases. With the developments reported here the chemical composition of secondary minerals can be analysed *in situ*, along with the composition of the neighbouring, primary mineral. This approach allows to study isotopic fractionation on a µm scale and relate the observed fractionation factors to the chemical composition of the phases involved. The method can also be applied to other metal stable isotope such as Mg and Fe, for example, and to other sample types, such as meteorites, igneous rocks or biogenic silica. LASS-ICP-MS could be further extended to use more

than two instruments simultaneously, e.g. a MC-ICP-MS for high precision isotope ratios, a sector field-ICP-MS for radiogenic isotope ratios and a fast scanning quadrupole ICP-MS or ICP-TOFMS for the major element composition of a sample.

For specialised applications, such as the simultaneous determination of $\delta^{11}B$ and B/Ca in foraminifera using matrix matched standards[20], LA-MC-ICP-MS|OES is a good and convenient alternative to LASS-ICP-MS. We are currently exploring to increase the sensitivity of rear-on OES. With this modification, the method could also be applied as a routine quality control for solution isotope ratio measurements. The analyte solution which was previously separated from the matrix could be routinely monitored for its purity. Thus differences between the compositions of a sample and a bracketing standard that might compromise the external mass bias correction approach could be detected and thereby adding another decisive control to produce high accurate isotope ratio data.

## 5. Conclusion

The combinations of laser ablation split stream ICP-MS with a multicollector ICP-MS (LASS-ICP-MS) and optical emission spectroscopy of the LA-MC-ICP-MS plasma (LA-MC-ICP-MS|OES) are versatile tools for simultaneous investigating the isotopic and chemical composition, without a compromise on the accuracy and precision of the silicon isotope ratio determinations. Quantification of major and trace element composition down to the µg $g^{-1}$ level were achieved applying LASS-ICP-MS and using an internal standard or a 100 wt% oxide normalisation approach. A direct comparison with previous work on the analytical performance of pumped LASS cannot be easily achieved, due to the lack of published performance data and application of fs-LASS-ICP-MS. We estimated to achieve with the current pumped split approximately 25% of the sensitivity that is achievable using direct fs-LA-ICP-MS, and thus also increasing the limits of detection by a factor of 4.

The analytical challenge for this type of combined analysis is clearly the stable metal isotope ratio analysis. Whereas the determination of elemental concentrations in this study only failed where signal intensity dropped below the background, the stable Si isotope analysis is much more sensitive to the instrumental setup. The challenge is to obtain stable operating conditions of the MC-ICP-MS despite partitioning a part of the aerosol into the second instrument. This stability is required to minimise mass bias drift between the bracketing standards and to attain stable conditions to reliably resolve isobaric interferences on Si isotopes over long measurement sequences. Optimisation of the MC-ICP-MS is thus the first priority. A stable, but flexible tuning of the amount of laser aerosol introduced by a pumped split stream approach ensures implementing this priority. Following these suggestions we find that stable silicon isotope ratios obtained by LASS-ICP-MS show no difference in their accuracy and precision to non-LASS results reported previously.[10]

Rear-on optical emission spectroscopy (OES) can be used to determine major elements in geological samples. The method is, however, compromised by high limits of detection. In the currently applied setup it is thus not the preferred method for routine trace element analysis of mineral phases.

Our preferred method for the simultaneous isotopic and element composition analysis is LASS in combination with a quadrupole and multicollector ICP-MS. This combination offers a big advantage for Si isotope analysis of unknown mineral phases, where knowledge of their chemical composition would else require laborious application of other microanalytical methods such as EMPA, EDX, or SIMS.

## Acknowledgments

This work is a contribution from the Marie Curie Initial Training Network IsoNose (www.IsoNose.eu) that is funded by the People Programme (Marie Curie Actions) of the European Union's Seventh Framework Programme FP7/2007-2013/ under REA grant agreement n° [608069]. The research was carried out in the Helmholtz Laboratory for the Geochemistry of the Earth Surface at GFZ Potsdam. The authors thank Josefine Buhk for the support with the set-up of the light collection optical emission spectroscopy. The authors would like to thank two anonymous reviewers for their constructive comments that greatly improved the manuscript. D. A. F. would like to thank Marcus Oelze and Michael

Tatzel for the discussions of this manuscript and Reto Glaus for the discussions concerning LIBS and light collection OES.

## References

[1] C.M. Johnson, B.L. Beard, F. Albarede, Overview and General Concepts, Rev. Mineral. Geochemistry. 55 (2004) 1–24. doi:10.2138/gsrmg.55.1.1.

[2] T.D. Bullen, A. Eisenhauer, Metal stable isotopes in low-temperature systems: A primer, Elements. 5 (2009) 349–352. doi:10.2113/gselements.5.6.349.

[3] R. Chakrabarti, Silicon isotopes: From cosmos to benthos, Curr. Sci. 108 (2015) 246–254.

[4] P.S. Savage, R.M.G. Armytage, R.B. Georg, A.N. Halliday, High temperature silicon isotope geochemistry, Lithos. 190-191 (2014) 500–519. doi:10.1016/j.lithos.2014.01.003.

[5] P.J. Frings, W. Clymans, G. Fontorbe, C.L. De La Rocha, D.J. Conley, The continental Si cycle and its impact on the ocean Si isotope budget, Chem. Geol. 425 (2016) 12–36. doi:10.1016/j.chemgeo.2016.01.020.

[6] K. Ziegler, E.D. Young, E.A. Schauble, J.T. Wasson, Metal–silicate silicon isotope fractionation in enstatite meteorites and constraints on Earth's core formation, Earth Planet. Sci. Lett. 295 (2010) 487–496. doi:10.1016/j.epsl.2010.04.030.

[7] S. Opfergelt, P. Delmelle, Silicon isotopes and continental weathering processes: Assessing controls on Si transfer to the ocean, Comptes Rendus - Geosci. 344 (2012) 723–738. doi:10.1016/j.crte.2012.09.006.

[8] J. Chmeleff, I. Horn, G. Steinhoefel, F. von Blanckenburg, In situ determination of precise stable Si isotope ratios by UV-femtosecond laser ablation high-resolution multi-collector ICP-MS, Chem. Geol. 249 (2008) 155–166. doi:10.1016/j.chemgeo.2007.12.003.

[9] G. Steinhoefel, J. Breuer, F. von Blanckenburg, I. Horn, D. Kaczorek, M. Sommer, Micrometer silicon isotope diagnostics of soils by UV femtosecond laser ablation, Chem. Geol. 286 (2011) 280–289. doi:10.1016/j.chemgeo.2011.05.013.

[10] J.A. Schuessler, F. von Blanckenburg, Testing the limits of micro-scale analyses of Si stable isotopes by femtosecond laser ablation multicollector inductively coupled plasma mass spectrometry with application to rock weathering, Spectrochim. Acta Part B At. Spectrosc. 98 (2014) 1–18. doi:10.1016/j.sab.2014.05.002.

[11] M. Wiedenbeck, L.P. Bédard, R. Bugoi, M. Horan, K. Linge, S. Merchel, L.F.G. Morales, D. Savard, a. K. Souders, P. Sylvester, GGR Biennial Critical Review: Analytical Developments Since 2012, Geostand. Geoanalytical Res. 38 (2014) 467–512. doi:10.1111/j.1751-908X.2014.00347.x.

[12] A.L. Gray, Solid sample introduction by laser ablation for inductively coupled plasma source mass spectrometry, Analyst. 110 (1985) 551. doi:10.1039/an9851000551.

[13] D. Günther, B. Hattendorf, Solid sample analysis using laser ablation inductively coupled plasma mass spectrometry, TrAC Trends Anal. Chem. 24 (2005) 255–265. doi:10.1016/j.trac.2004.11.017.

[14] B.J. Fryer, S.E. Jackson, H.P. Longerich, Design, operation and role of the laser-ablation microprobe coupled with an inductively coupled plasma - mass spectrometer (LAM-ICP-MS) in the Earth sciences, Can. Mineral. 33 (1995) 303–312.

[15] A. Shahar, E. Young, Astrophysics of CAI formation as revealed by silicon isotope LA-MC-ICPMS of an igneous CAI, Earth Planet. Sci. Lett. 257 (2007) 497–510. doi:10.1016/j.epsl.2007.03.012.

[16] R.E. Russo, X. Mao, S.S. Mao, The Physics of Laser Ablation in Microchemical Analysis, Anal. Chem. 74 (2002) 70 A–77 A. doi:10.1021/ac0219445.

[17] H. Wiltsche, D. Günther, Capabilities of femtosecond laser ablation ICP-MS for the major, minor, and trace element analysis of high alloyed steels and super alloys, Anal. Bioanal. Chem. 399 (2011) 2167–2174. doi:10.1007/s00216-010-4605-8.

[18] H.L. Yuan, S. Gao, M.N. Dai, C.L. Zong, D. Günther, G.H. Fontaine, X.M. Liu, C. Diwu, Simultaneous determinations of U-Pb age, Hf isotopes and trace element compositions of zircon by excimer laser-ablation quadrupole and multiple-collector ICP-MS, Chem. Geol. 247 (2008) 100–118. doi:10.1016/j.chemgeo.2007.10.003.

[19] C. Latkoczy, T. Ghislain, Simultaneous LIBS and LA-ICP-MS analysis of industrial samples, J. Anal. At. Spectrom. 21 (2006) 1152. doi:10.1039/b607697c.

[20] K. Kaczmarek, I. Horn, G. Nehrke, J. Bijma, Simultaneous determination of δ11B and B/Ca ratio in marine biogenic carbonates at nanogram level, Chem. Geol. 392 (2014) 32–42. doi:10.1016/j.chemgeo.2014.11.011.

[21] K. G. Heumann, S. M. Gallus, G. Rädlinger, J. Vogl, Precision and accuracy in isotope ratio measurements by plasma source mass spectrometry, J. Anal. At. Spectrom. 13 (1998) 1001. doi:10.1039/a801965g.

[22] O. Borovinskaya, B. Hattendorf, M. Tanner, S. Gschwind, D. Günther, A prototype of a new inductively coupled plasma time-of-flight mass spectrometer providing temporally resolved, multi-element detection of short signals generated by single particles and droplets, J. Anal. At. Spectrom. 28 (2013) 226–233. doi:10.1039/C2JA30227F.

[23] D. Ardelt, A. Polatajko, O. Primm, M. Reijnen, Isotope ratio measurements with a fully simultaneous Mattauch-Herzog ICP-MS, Anal. Bioanal. Chem. 405 (2013) 2987–2994. doi:10.1007/s00216-012-6543-0.

[24] M. Resano, K.S. McIntosh, F. Vanhaecke, Laser ablation-inductively coupled plasma-mass spectrometry using a double-focusing sector field mass spectrometer of Mattauch-Herzog geometry and an array detector for the determination of platinum group metals and gold in NiS buttons obtained by fire as, J. Anal. At. Spectrom. 27 (2012) 165–173. doi:10.1039/c1ja10193e.

[25] A.R.C. Kylander-Clark, B.R. Hacker, J.M. Cottle, Laser-ablation split-stream ICP petrochronology, Chem. Geol. 345 (2013) 99–112. doi:10.1016/j.chemgeo.2013.02.019.

[26] D.W. Hahn, N. Omenetto, Laser-Induced Breakdown Spectroscopy (LIBS), Part II: Review of Instrumental and Methodological Approaches to Material Analysis and Applications to Different Fields, Appl. Spectrosc. 66 (2012) 347–419. doi:10.1366/11-06574.

[27] J.R. Chirinos, D.D. Oropeza, J.J. Gonzalez, H. Hou, M. Morey, V. Zorba, R.E. Russo, Simultaneous 3-dimensional elemental imaging with LIBS and LA-ICP-MS, J. Anal. At. Spectrom. 29 (2014) 1292. doi:10.1039/c4ja00066h.

[28] P.E. Janney, F.M. Richter, R.A. Mendybaev, M. Wadhwa, R.B. Georg, E.B. Watson, R.R. Hines, Matrix effects in the analysis of Mg and Si isotope ratios in natural and synthetic glasses by laser ablation-multicollector ICPMS: A comparison of single- and double-focusing mass spectrometers, Chem. Geol. 281 (2011) 26–40. doi:10.1016/j.chemgeo.2010.11.026.

[29] J. Koch, M. Wälle, J. Pisonero, D. Günther, Performance characteristics of ultra-violet femtosecond laser ablation inductively coupled plasma mass spectrometry at ~265 and ~200 nm, J. Anal. At. Spectrom. 21 (2006) 932. doi:10.1039/b603929d.

[30] S.M. Eggins, L.P.J. Kinsley, J.M.G. Shelley, Deposition and element fractionation processes during atmospheric pressure laser sampling for analysis by ICP-MS, Appl. Surf. Sci. 127-129 (1998) 278–286. doi:10.1016/S0169-4332(97)00643-0.

[31] D. Günther, C.A. Heinrich, Enhanced sensitivity in laser ablation-ICP mass spectrometry using helium-argon mixtures as aerosol carrier, J. Anal. At. Spectrom. 14 (1999) 1363–1368.

doi:10.1039/a901648a.

[32] C. O'Connor, B.L. Sharp, P. Evans, On-line additions of aqueous standards for calibration of laser ablation inductively coupled plasma mass spectrometry: theory and comparison of wet and dry plasma conditions, J. Anal. At. Spectrom. 21 (2006) 556. doi:10.1039/b600916f.

[33] F. Claverie, B. Fernández, C. Pécheyran, J. Alexis, O.F.X. Donard, Elemental fractionation effects in high repetition rate IR femtosecond laser ablation ICP-MS analysis of glasses, J. Anal. At. Spectrom. 24 (2009) 891. doi:10.1039/b904134f.

[34] L. Flamigni, J. Koch, D. Günther, The effect of carrier gas humidity on the vaporization of laser-produced aerosols in inductively coupled plasmas, J. Anal. At. Spectrom. 29 (2014) 280–286. doi:10.1039/C3JA50314C.

[35] L. Flamigni, J. Koch, D. Günther, Experimental and theoretical investigations about the vaporization of laser-produced aerosols and individual particles inside inductively-coupled plasmas - Implications for the extraction efficiency of ions prior to mass spectrometry, Spectrochim. Acta - Part B At. Spectrosc. 76 (2012) 70–76. doi:10.1016/j.sab.2012.07.016.

[36] R. Glaus, L. Dorta, Z. Zhang, Q. Ma, H. Berke, D. Günther, Isotope ratio determination of objects in the field by portable laser ablation sampling and subsequent multicollector ICPMS, J. Anal. At. Spectrom. 28 (2013) 801. doi:10.1039/c3ja30379a.

[37] K.P. Jochum, U. Weis, B. Stoll, D. Kuzmin, Q. Yang, I. Raczek, D.E. Jacob, A. Stracke, K. Birbaum, D.A. Frick, D. Günther, J. Enzweiler, Determination of Reference Values for NIST SRM 610-617 Glasses Following ISO Guidelines, Geostand. Geoanalytical Res. 35 (2011) 397–429. doi:10.1111/j.1751-908X.2011.00120.x.

[38] K.P. Jochum, U. Nohl, K. Herwig, E. Lammel, B. Stoll, A.W. Hofmann, GeoReM: A New Geochemical Database for Reference Materials and Isotopic Standards, Geostand. Geoanalytical Res. 29 (2005) 333–338. doi:10.1111/j.1751-908X.2005.tb00904.x.

[39] M.B. Fricker, Design of ablation cells for LA-ICP-MS, ETH Zürich, 2012. doi:10.3929/ethz-a-007615617.

[40] H.P. Longerich, S.E. Jackson, D. Günther, Laser ablation inductively coupled plasma mass spectrometric transient signal data acquisition and analyte concentration calculation, J. Anal. At. Spectrom. 11 (1996) 899–904. doi:10.1039/Ja9961100899.

[41] Y. Liu, Z. Hu, S. Gao, D. Günther, J. Xu, C. Gao, H. Chen, In situ analysis of major and trace elements of anhydrous minerals by LA-ICP-MS without applying an internal standard, Chem. Geol. 257 (2008) 34–43. doi:10.1016/j.chemgeo.2008.08.004.

[42] F. Albarede, B. Beard, Analytical Methods for Non-Traditional Isotopes, Rev. Mineral. Geochemistry. 55 (2004) 113–152. doi:10.2138/gsrmg.55.1.113.

[43] T.B. Coplen, J. a Hopple, J.K. Böhlke, H.S. Peiser, S.E. Rieder, H.R. Krouse, K.J.R. Rosman, T. Ding, R.D.J. Vocke, K.M. Révész, A. Lamberty, P. Taylor, P. De Bièvre, Compilation of minimum and maximum isotope ratios of selected elements in naturally occurring terrestrial materials and reagents, U.S. Geol. Surv. Water-Resources Investig. Rep. 01-4222. (2002) 45–50. http://pubs.usgs.gov/wri/wri014222/.

[44] A.Y. Borisova, R. Freydier, M. Polvé, K.P. Jochum, F. Candaudap, Multi-elemental analysis of ATHO-G rhyolitic glass (MPI-DING reference material) by femtosecond and nanosecond LA-ICP-MS: Evidence for significant heterogeneity of B, V, Zn, Mo, Sn, Sb, Cs, W, Pt and Pb at the millimetre scale, Geostand. Geoanalytical Res. 34 (2010) 245–255. doi:10.1111/j.1751-908X.2010.00077.x.

## Figures

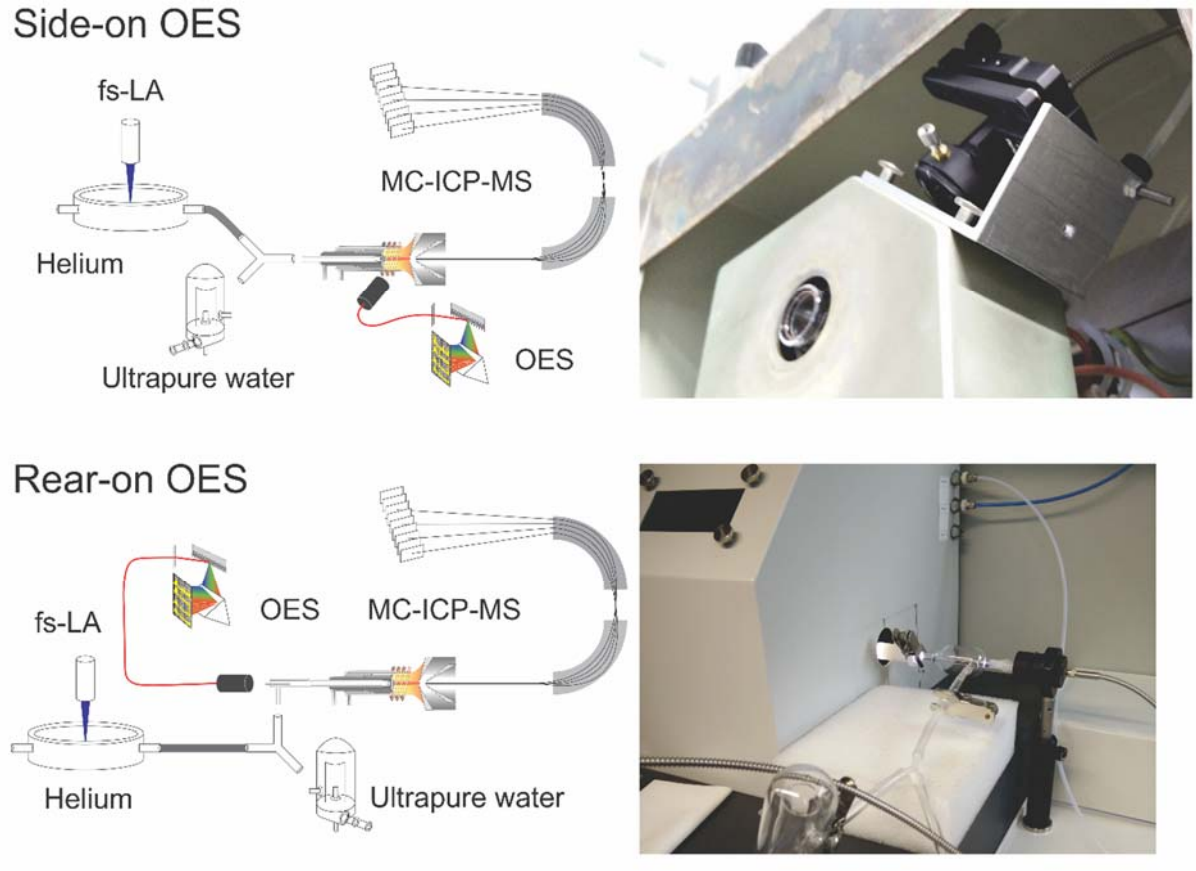


*Figure 1: Set-up for the side-on (top) and rear-on (bottom) optical emission spectroscopy (OES) in combination with simultaneous isotope ratio measurement on the multicollector. The light of the plasma of the MC-ICP-MS is guided into the OES using a fibre bundle (red).*

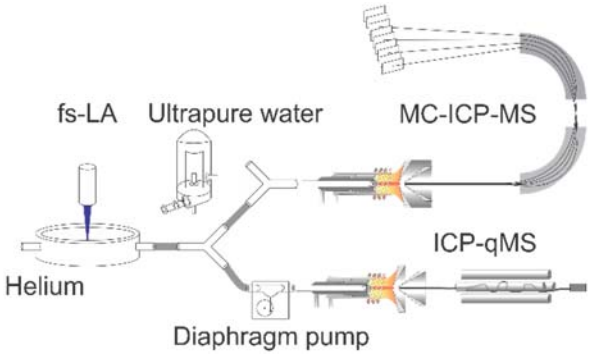


*Figure 2: Schematics of the laser ablation split stream (LASS-ICP-MS) set-up. The laser aerosol is split using a Y-piece and is transported into the MC-ICP-MS and into the quadrupole ICP-MS, whereas the latter transport path is actively pumped using a diaphragm pump.*

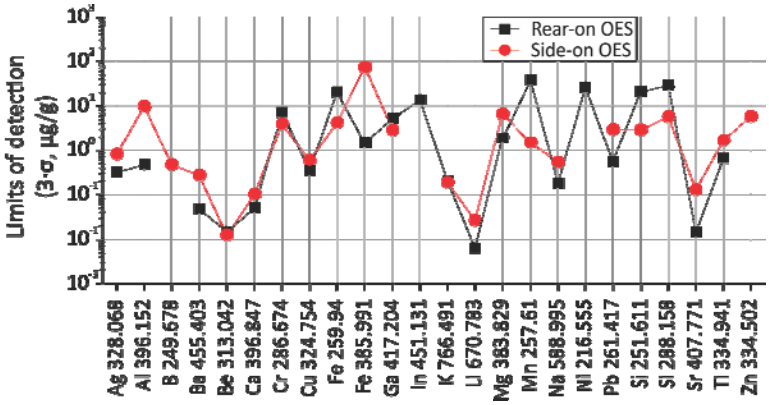


*Figure 3: Comparison of limits of detection for concentration measurements in µg $g^{-1}$ between rear-on and side-on optical emission spectroscopy using solution nebulisation under laser ablation conditions. For values not shown, no significant signal above background was detected.*

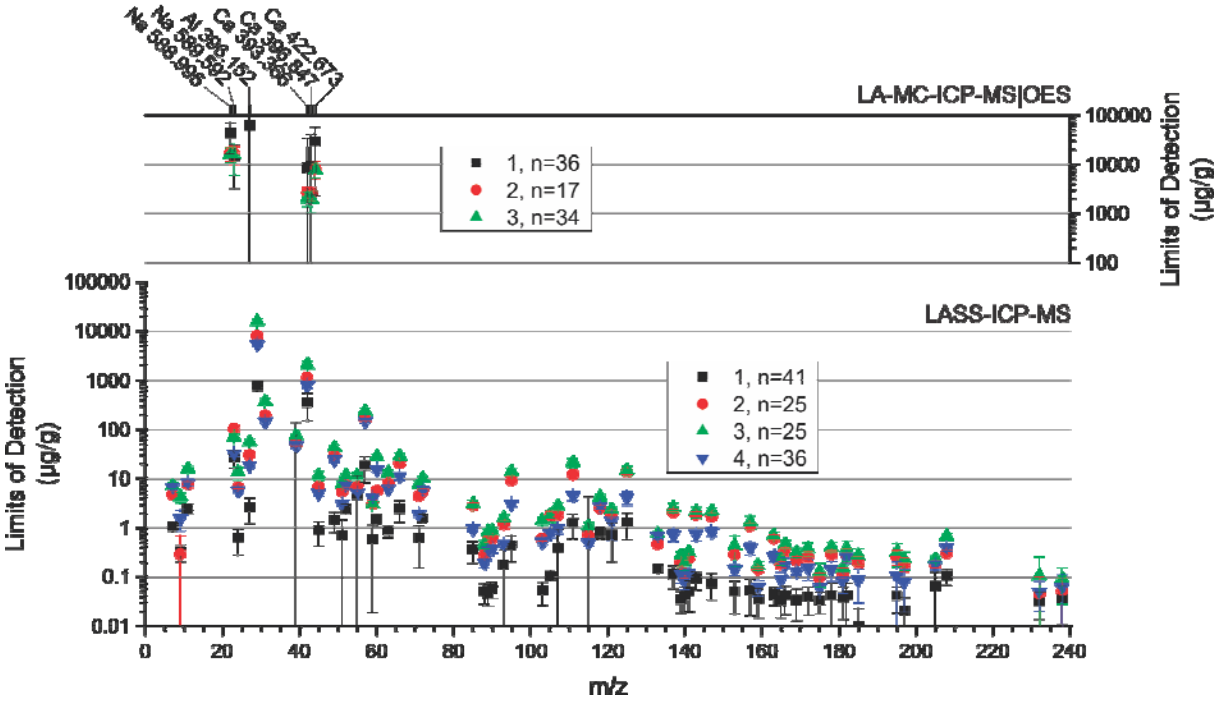


*Figure 4: Comparison of limits of detection (in µg $g^{-1}$) between rear-on LA-MC-ICP-MS|OES and LASS-ICP-MS based on 3-times the standard deviation of the gas background, determined on NIST SRM610. For LA-MC-ICP-MS|OES only Na, Al and Ca are above the background, whereas for LASS-ICP-MS all elements detectable by ICP mass spectrometry can be determined in the µg $g^{-1}$ to sub-µg $g^{-1}$ level. Numbers indicate the analytical session, error bars are 1 SD based on replicated LOD determinations, n number of replicates.*

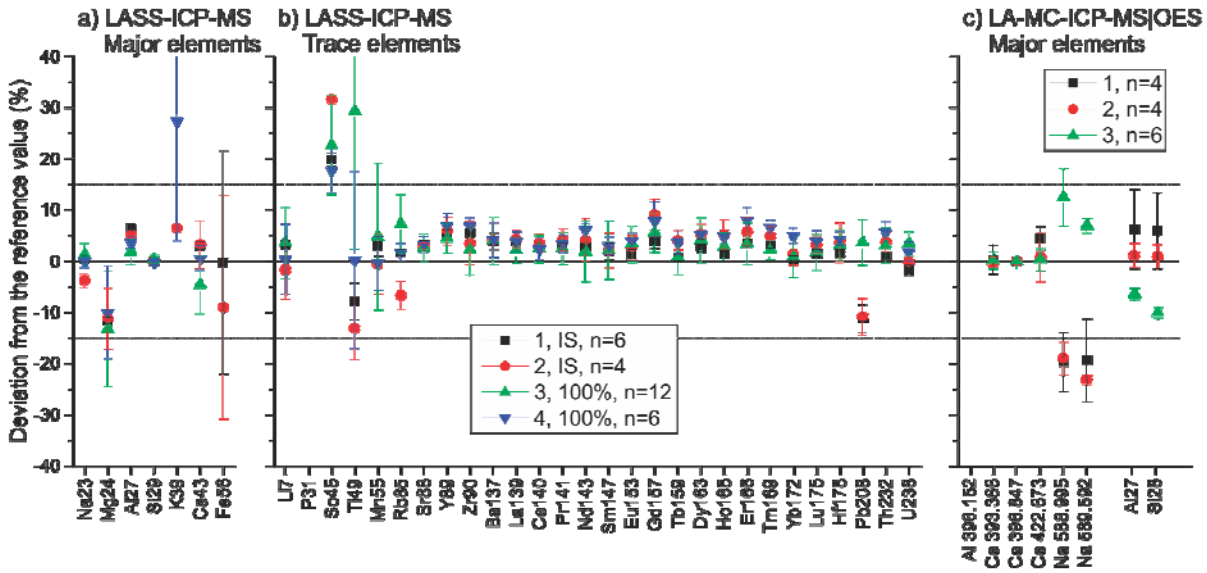


*Figure 5: Relative deviation from the reference value for repeated NIST SRM612 determination of major (panel a) and trace elements (panel b) by LASS-ICP-MS. Element concentration were calculated by two methods: IS, using an internal standard ($^{29}$Si), or 100%, normalising all elements to 100 wt% oxides. Panel c: rear-on LA-MC-ICP-MS|OES using Ca (396.847 nm) as internal standard. NIST SRM610 was used as external standard. For LASS-ICP-MS, the observed deviations from reference values are typically smaller than 10-15% relative, whereas for rear-on OES elevated deviation for Na (20-25%) was observed. LASS-ICP-MS data are from four and rear-on OES from three independent analytical sessions, n indicates the number of replicated measurements during the analytical sessions.*

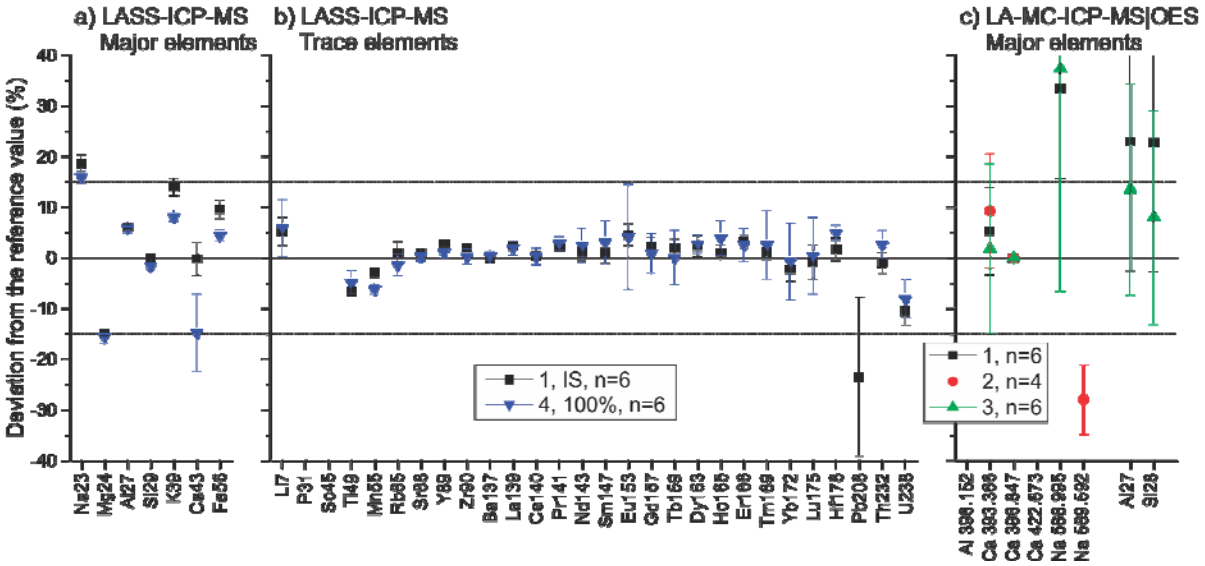


*Figure 6: Relative deviation from the reference value for repeated ATHO-G determination for major (panel a) and trace elements (panel b) by LASS-ICP-MS. Element concentration were calculated by two methods: IS, using an internal standard ($^{29}$Si), or 100%, normalising all elements to 100 wt% oxides. Panel c: rear-on LA-MC-ICP-MS|OES using Ca (396.847 nm) as internal standard. NIST SRM610 was used as external standard. For LASS-ICP-MS deviations are typically smaller than 10-15%, higher deviation was observed for Pb due to the low concentration in ATHO-G. For rear-on LA-MC-ICP-MS|OES elevated deviation for Na, Al and Si (20-25%) was observed. LASS-ICP-MS data are from two and rear-on LA-MC-ICP-MS|OES from three independent analytical sessions, n indicates the number of replicated measurements during the analytical sessions.*

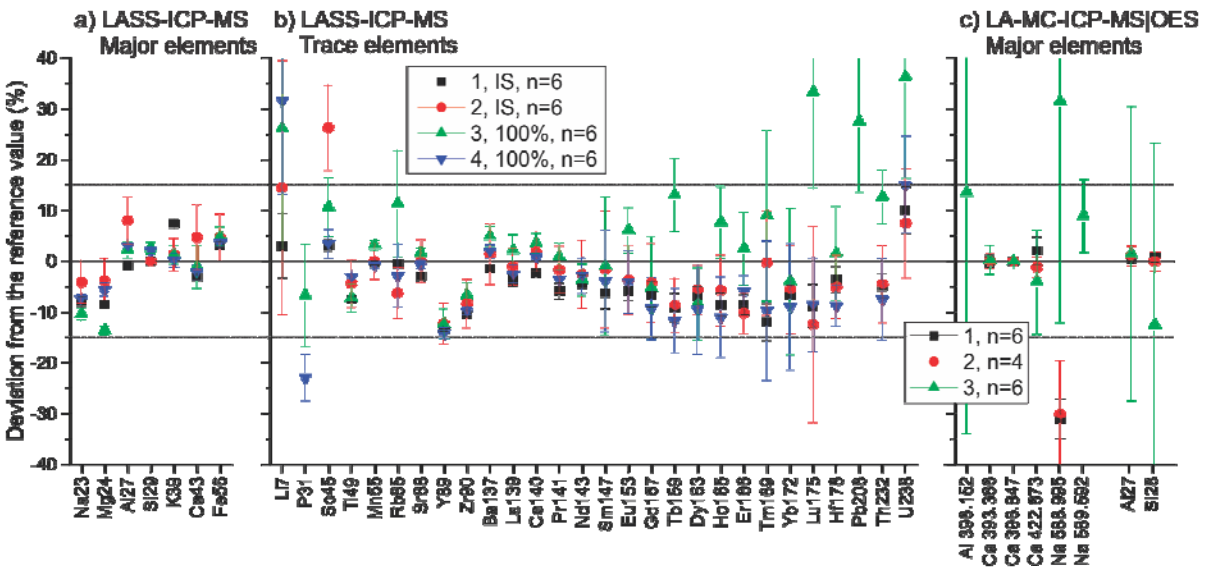


*Figure 7: Relative deviation from the reference value for repeated BHVO-2G determination for major (panel a) and trace elements (panel b) by LASS-ICP-MS. Element concentration were calculated by two methods: IS, using an internal standard ($^{29}$Si), or 100%, normalising all elements to 100 wt% oxides. Panel c: rear-on LA-MC-ICP-MS|OES using Ca (396.847 nm) as internal standard. NIST SRM610 was used as external standard. For LASS deviation are typically smaller than 10-15%, for low concentrated elements (< 10 µg g$^{-1}$) higher deviation are observed using the 100 wt% oxide normalisation approach. For rear-on OES elevated deviation for Na (30-35%) was observed. LASS data are from four and rear-on OES from three independent analytical sessions, n indicates the number of replicated measurements during the analytical sessions.*

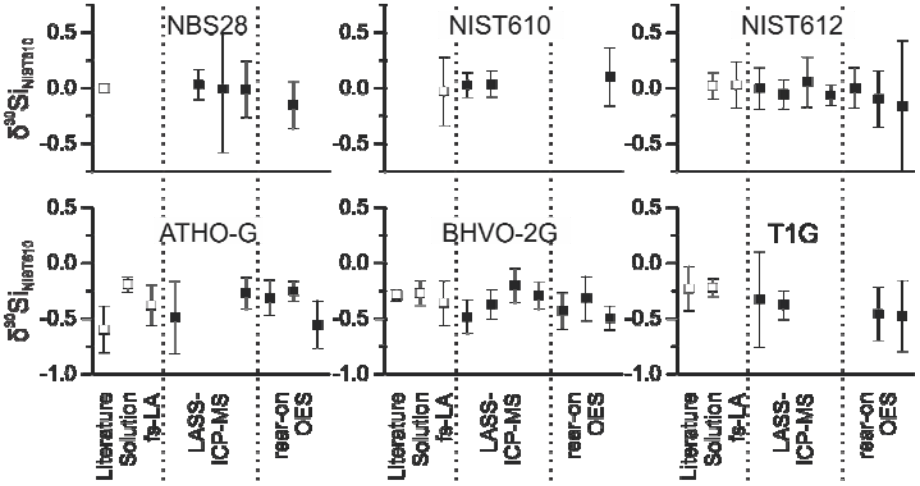


*Figure 8: Measured $\delta^{30}$Si (closed symbols) using NIST SRM610 as bracketing standard. Literature data (open symbols) as compiled from solution and fs-LA data, from Schuessler and von Blanckenburg.*[10]

## Tables

*Table 1: Overview of reference materials analysed for this study and published major composition (in wt%) and $\delta^{30}$Si (in ‰ relative to NBS28) values from the GeoReM Database*[38]. **For BHVO-2G the $\delta^{30}$Si values of BHVO-2 are shown.*

| | Material | Supplier | Major Composition [wt%] | Reported $\delta^{30}$Si range [‰] |
|---|---|---|---|---|
| **ATHO-G** | rhyolite glass | MPI | 12.2% $Al_2O_3$, 1.7% CaO, 3.27% FeO, 2.64% $K_2O$, 0.103% MgO, 3.75% $Na_2O$, 75.6% $SiO_2$, 0.255% $TiO_2$ | -0.60 to -0.19 ‰ |
| **BHVO-2G*** | basalt glass | USGS | 13.6% $Al_2O_3$, 11.4% CaO, 11.3% FeO, 0.51% $K_2O$, 7.13% MgO, 2.4% $Na_2O$, 49.3% $SiO_2$, 2.79% $TiO_2$ | -0.36 to -0.27 ‰ |

| | | | | |
|---|---|---|---|---|
| **GOR128-G** | komatiite glass | MPI | 9.91 $Al_2O_3$, 6.24% CaO, 9.81% FeO, 26% MgO, 0.574% $Na_2O$, 46.1% $SiO_2$, 0.288% $TiO_2$ | -0.46 ‰ |
| **IRMM 017** | silicon | IRMM | 100% Si | -1.36 to -1.22 ‰ |
| **NBS28** | quartz sand | NIST | 100% $SiO_2$ | ≡ 0 ‰ |
| **NIST SRM 610** | silicate glass | NIST | 1.95% $Al_2O_3$, 11.4% CaO, 13.4% $Na_2O$, 69.7% $SiO_2$ | -0.03‰ |
| **NIST SRM612** | silicate glass | NIST | 2.03% $Al_2O_3$, 11.9% CaO, 13.7% $Na_2O$, 72.1% $SiO_2$ | -0.07 to -0.03 ‰ |
| **T1-G** | diorite glass | MPI | 17.1% $Al_2O_3$, 7.1% CaO, 6.44% FeO, 1.96% $K_2O$, 3.75% MgO, 3.13% $Na_2O$, 58.6% $SiO_2$, 0.755% $TiO_2$ | -0.22 to -0.23‰ |

*Table 2: Si isotope data analysed by fs-LASS-MC-ICP-MS and fs-LA-MC-ICP-MS with rear-on OES. $\delta^{29}Si$ and $\delta^{30}Si$ are reported relative to NIST SRM610. Four respectively three analytical sessions were combined.*

| | **LASS-ICP-MS** | | | | | **Rear-on LA-MC-ICP-MS\|OES** | | | | |
|---|---|---|---|---|---|---|---|---|---|---|
| | $\delta^{29}Si$ | 2 SD | $\delta^{30}Si$ | 2 SD | n | $\delta^{29}Si$ | 2 SD | $\delta^{30}Si$ | 2 SD | n |
| | ‰ | ‰ | ‰ | ‰ | | ‰ | ‰ | ‰ | ‰ | |
| **ATHO-G** | -0.18 | 0.18 | -0.38 | 0.33 | 12 | -0.19 | 0.16 | -0.40 | 0.33 | 14 |
| **BHVO-2G** | -0.16 | 0.16 | -0.34 | 0.25 | 23 | -0.21 | 0.10 | -0.41 | 0.20 | 13 |
| **GOR128-G** | -0.14 | 0.08 | -0.19 | 0.09 | 5 | -0.23 | 0.12 | -0.42 | 0.12 | 4 |
| **IRMM017** | -0.64 | 0.07 | -1.27 | 0.22 | 16 | -0.66 | 0.10 | -1.29 | 0.26 | 6 |
| **ML3B** | - | - | - | - | - | -0.16 | 0.12 | -0.45 | 0.17 | 4 |
| **NBS28** | -0.02 | 0.17 | 0.01 | 0.35 | 18 | -0.06 | 0.06 | -0.15 | 0.21 | 3 |
| **NIST610** | 0.01 | 0.10 | 0.03 | 0.11 | 11 | 0.02 | 0.09 | 0.10 | 0.26 | 8 |
| **NIST612** | -0.02 | 0.14 | 0.00 | 0.20 | 31 | -0.05 | 0.17 | -0.09 | 0.42 | 14 |
| **T1-G** | -0.16 | 0.19 | -0.35 | 0.30 | 8 | -0.26 | 0.09 | -0.47 | 0.27 | 12 |

# Supplementary Information

## Instrument settings

*Table S1: Typical laser settings used throughout the study, laser repetition rate was adjusted to result in similar $^{28}Si$ intensities on the multicollector.*

| | | |
|---|---|---|
| Crater Diameter | 25-30 | [µm] |
| Repetition Rate | 20-80 | [Hz] |
| Scan Velocity | 40 | [µm/s] |
| Output Energy | 7-8 | [mW] |
| Wavelength | 196 | [nm] |
| Raster | 100x50 | [µm] |
| Passes | 10 | |

*Table S2: Neptune cup configuration with the used $10^{11}$ Ω amplifiers.*

| L4 | L3 | L2 | L1 | C | H1 | H2 | H3 | H4 |
|---|---|---|---|---|---|---|---|---|
| $^{27}Al$ | | $^{28}Si$ | | $^{29}Si$ | | $^{30}Si$ | | |
| $10^{11}$ Ω | | $10^{11}$ Ω | | $10^{11}$ Ω | | $10^{11}$ Ω | | |

*Table S3 Neptune MC-ICP-MS and laser settings used for the side-on and rear-on LA-MC-ICP-MS|OES. Gas flows are typically within 0.1 L min$^{-1}$ between analytical sessions.*

| | | | | | |
|---|---|---|---|---|---|
| Cool Gas Flow | 15.00 | [L min$^{-1}$] | Extraction Lens | -2000 | [V] |
| Auxiliary Gas Flow | 0.63 | [L min$^{-1}$] | Focus Lens | -583 | [V] |
| Nebuliser Gas Flow | 0.569 | [L min$^{-1}$] | X-Deflection | -0.49 | [V] |
| Helium Gas Flow | 1.20 | [L min$^{-1}$] | Y-Deflection | -3.23 | [V] |
| RF Power | 1250 | [W] | Shape | 208 | [V] |
| X | 0.780 | [mm] | Rotation Quad 1 | 0.0 | [V] |
| Y | -3.320 | [mm] | Source Offset | -1.0 | [V] |
| Z | -0.940 | [mm] | Focus Quad 1 | -19.89 | [V] |
| | | | Rotation Quad 2 | 0.0 | [V] |
| Focus Quad | -0.7 | [V] | Focus Offset | 50 | [V] |
| Dispersion | 0.0 | [V] | Matsuda Plate | 0.0 | [V] |

*Table S4: Instrument settings used for simultaneous isotope and concentration measurements by LASS-ICP-Top: Neptune settings; bottom iCAP-Qc settings. Gas flows are typically within 0.1 L min$^{-1}$ between analytical sessions.*

| | | | | | |
|---|---|---|---|---|---|
| **Neptune** | | | | | |
| Cool Gas Flow | 15.00 | [L min$^{-1}$] | Extraction Lens | -2000 | [V] |
| Auxiliary Gas Flow | 0.60 | [L min$^{-1}$] | Focus Lens | -543 | [V] |
| Nebuliser Gas Flow | 0.569 | [L min$^{-1}$] | X-Deflection | -3.48 | [V] |
| Helium Gas Flow | 1.74 | [L min$^{-1}$] | Y-Deflection | -3.11 | [V] |
| RF Power | 1250 | [W] | Shape | 202.00 | [V] |
| X | 0.640 | [mm] | Rotation Quad 1 | 0.0 | [V] |
| Y | -3.330 | [mm] | Source Offset | -1.0 | [V] |
| Z | -0.940 | [mm] | Focus Quad 1 | -19.89 | [V] |
| | | | Rotation Quad 2 | 2.50 | [V] |
| Focus Quad | -0.7 | [V] | Focus Offset | 50 | [V] |
| Dispersion | 0.0 | [V] | Matsuda Plate | 0 | [V] |
| **iCAP-Qc** | | | | | |
| Cool Gas Flow | 14.00 | [L min$^{-1}$] | X | 0.77 | [mm] |
| Auxiliary Gas Flow | 0.5234 | [L min$^{-1}$] | Y | -0.57 | [mm] |

| | | | | | |
|---|---|---|---|---|---|
| Nebuliser Gas Flow | 0.5146 | [L min$^{-1}$] | Z | 4.0 | [mm] |
| RF Power | 1400 | [W] | Extraction Lens | -187.5 | [V] |
| | | | CCT Focus Lens | -0.51 | [V] |
| External Pump | 4.2 – 4.7 | [V] | Volume to iCAP | 0.3 – 0.35 | [L min$^{-1}$] |

## Script for transposing the exported OES CSV files

Csv2gnuplot.sh can be found at https://gist.github.com/1312337

```
echo "** Script for transposing files       **"
echo "** obtained from OES Worksheet File  **"
echo "** Exp. Settings: CSV/Wiederholungen **"
echo "** v1.5, DAF, GFZ-Potsdam 04/2015    **"
echo "  :::::::::      :::     ::::::::::   "
echo "  :+:    :+:   :+: :+:   :+:          "
echo "  +:+    +:+  +:+   +:+  +:+          "
echo "  +#+    +:+ +#++:++#++: :#::+::#     "
echo "  +#+    +#+ +#+     +#+ +#+          "
echo "  #+#    #+# #+#     #+# #+#          "
echo "  #########  ###     ### ###          "
echo "****************************************"
echo "Removing extra lines on results files..."
sed -i '1,1d' *.csv
sed -i 's/"//g' *.csv
echo "Splitting measurements in different files..."
echo "Number of measured wavelengths:"
read nbrlines;
echo "Prefix of Samples:"
read prefix;
for cfiles in *.csv
    do split -l "$nbrlines" "$cfiles" output;
    a=1;
    for i in output*
        do new="$prefix"-"$a";
        mv ${i} ${new}.dat;
        let a=a+1; done
    let runs=runs+1; done
echo "Transposing, make sure that csv2gnuplot.sh is present!"
for file in *.dat
    do g=${file%.dat};
       bash csv2gnuplot.sh -t -i "$file" -o "$g"t.gfz;  done
       rm *.dat;
echo "Removing Extra Lines..."
sed -i '2d' *.gfz;
sed -i '4,10d' *.gfz;
echo "Done."
```

## Comparison between rear-on LA-MC-ICP-MS|OES and LASS-ICP-MS

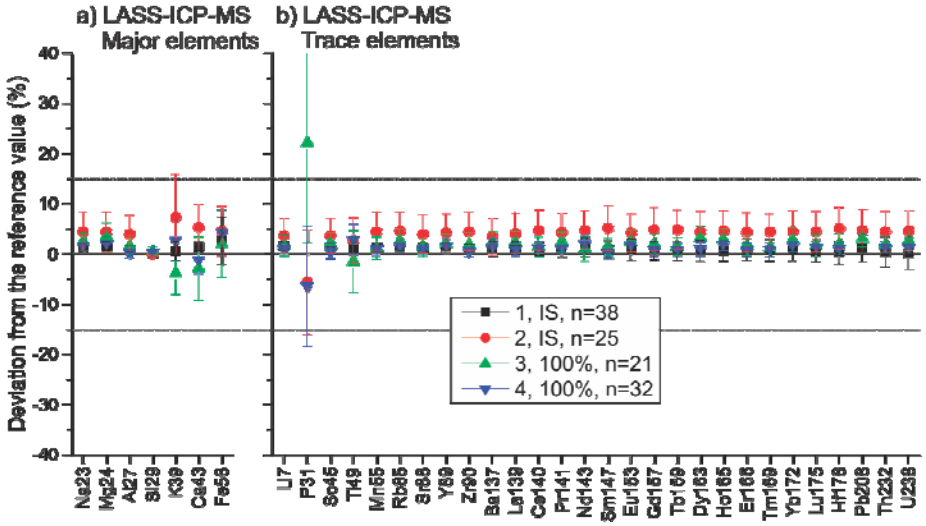


*Supporting Figure 1: Deviation from the reference value for NIST SRM610 for the major (panel a) and trace elements (panel b) determined by LASS-ICP-MS using an internal standard ($^{29}Si$, abbreviated IS) or 100 wt% oxide normalisation approach (abbreviated 100%), four independent analytical sessions, n indicates the number of replicated measurements during the analytical sessions. NIST SRM610 was used as external standard.*

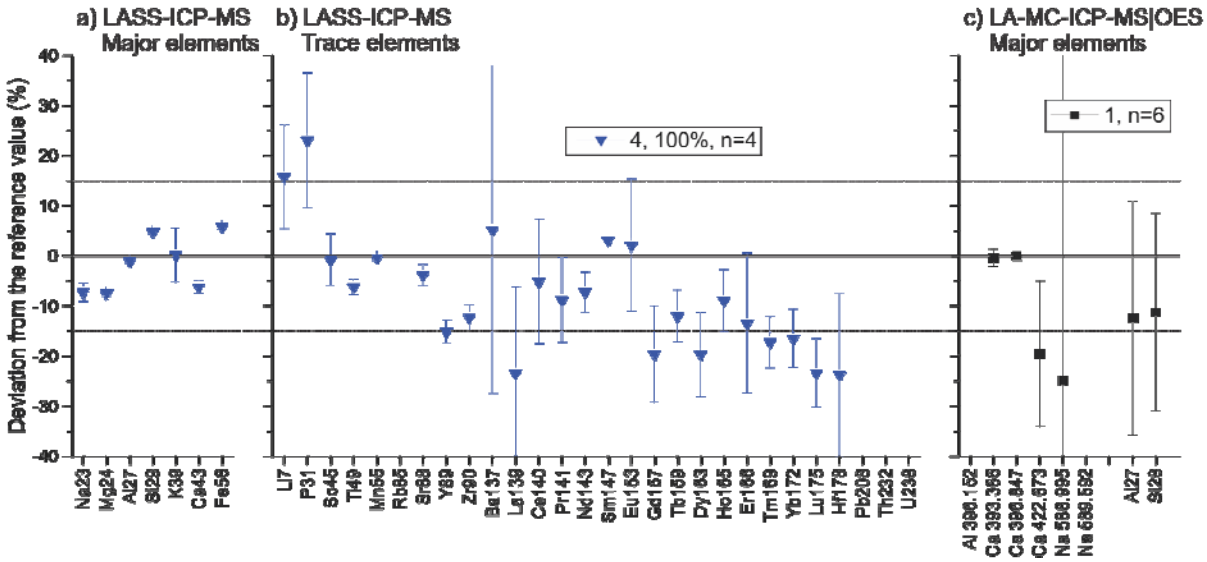


*Supporting Figure 2: Deviation from the reference value for repeated GOR128-B determination for major (panel a) and trace elements (panel b) by LASS-ICP-MS. Element concentration were calculated by two methods: IS, using an internal standard ($^{29}Si$), or 100%, normalising all elements to 100 wt% oxides. Panel c: rear-on LA-MC-ICP-MS|OES using Ca (396.847 nm) as internal standard. NIST SRM610 was used as external standard. NIST SRM610 was used as external standard. LASS-ICP-MS and rear-on LA-MC-ICP-MS|OES data are from one independent analytical sessions, n indicates the number of replicated measurements during the analytical sessions.*

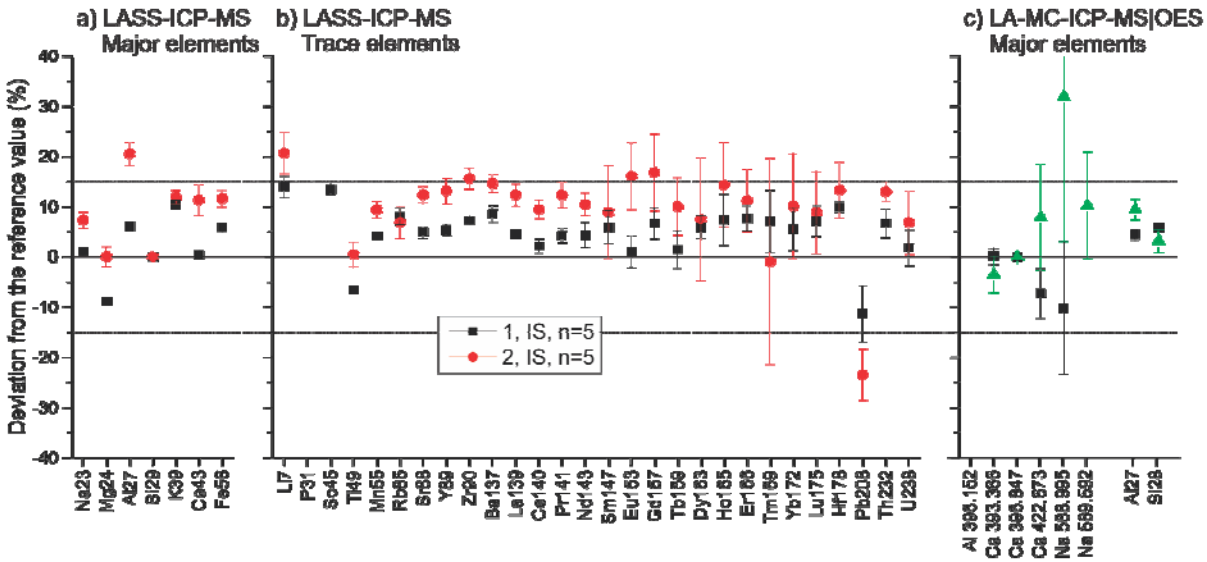


*Supporting Figure 3: Deviation from the reference value for repeated T1-G determination for major (panel a) and trace elements (panel b) by LASS-ICP-MS. Element concentration were calculated by two methods: IS, using an internal standard ($^{29}Si$), or 100%, normalising all elements to 100 wt% oxides. Panel c: rear-on LA-MC-ICP-MS|OES using Ca (396.847 nm) as internal standard. NIST SRM610 was used as external standard. NIST SRM610 was used as external standard. For LASS deviation are typically smaller than 10-15%, higher deviation for Pb due to low concentration in T1-G. For rear-on OES higher deviation for Na (20-25%) was observed. LASS data are from two and rear-on LA-MC-ICP-MS|OES from two independent analytical sessions, n indicates the number of replicated measurements during the analytical sessions.*

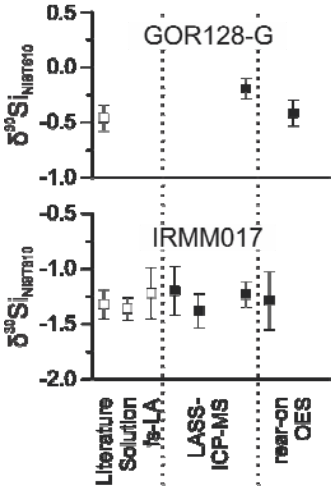


*Supporting Figure 4: Measured $\delta^{30}Si$ (closed symbols) using NIST SRM610 as bracketing standard. Literature data (open symbols) as compiled from solution and fs-LA data, from Schuessler and von Blanckenburg.*[10]